Supporting Information for

Possible gapless spin-liquid state in the Fe-based halide perovskite $Cs_4BiFeBr_{10}$ derived from antiferromagnet $CsFeBr_4$

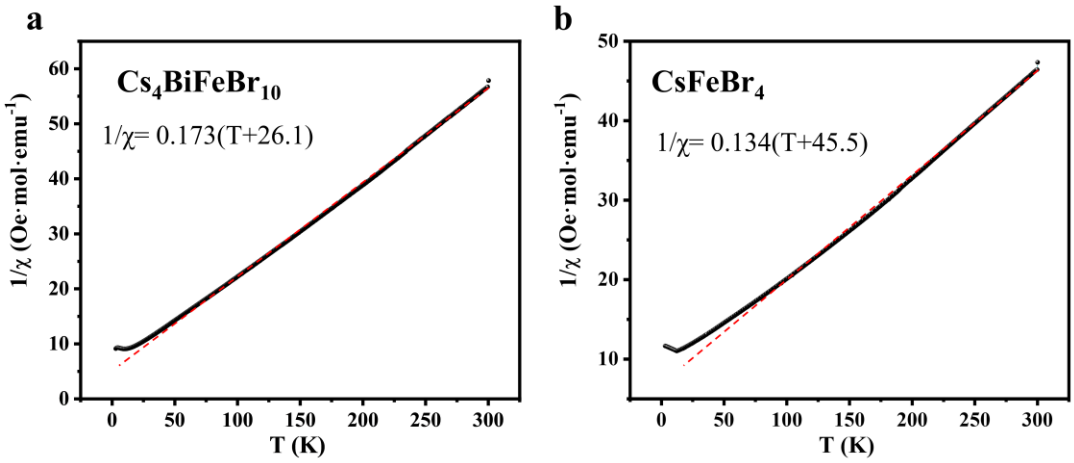

Figure S1. a and **b**, Curie-Wiess fitting of 1/χ-T curves for $Cs_4BiFeBr_{10}$ and $CsFeBr_4$ single crystals, respectively.

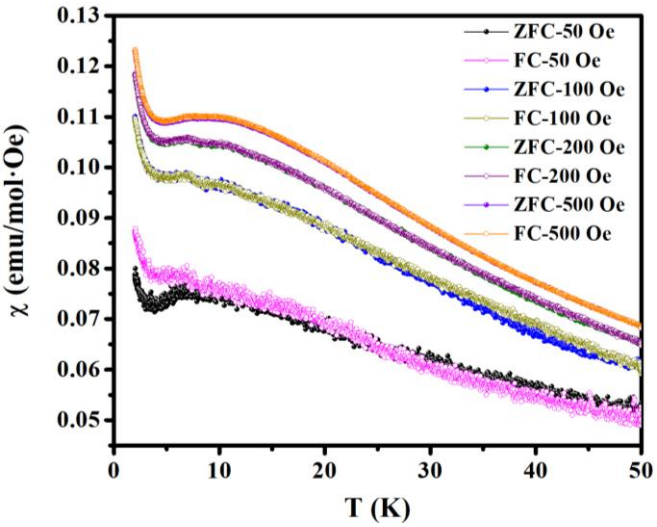

Figure S2. Temperature dependence of magnetic susceptibility for $Cs_4BiFeBr_{10}$.

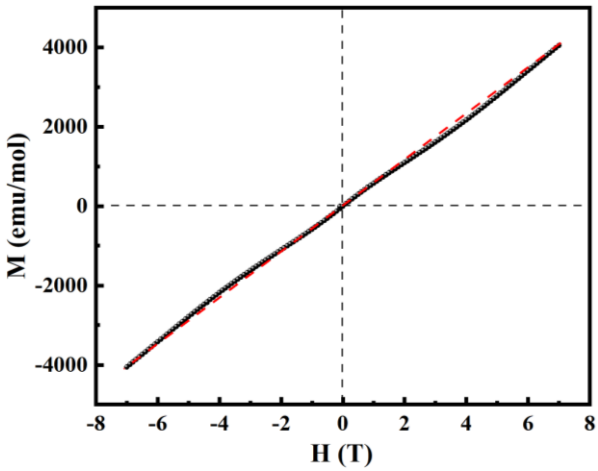

Figure S3. M-H curve cycle of $Cs_4BiFeBr_{10}$ single crystal at 2 K. The scanning process of the magnetic field: 0T→7T→0T→(-7T)→0T→7T.

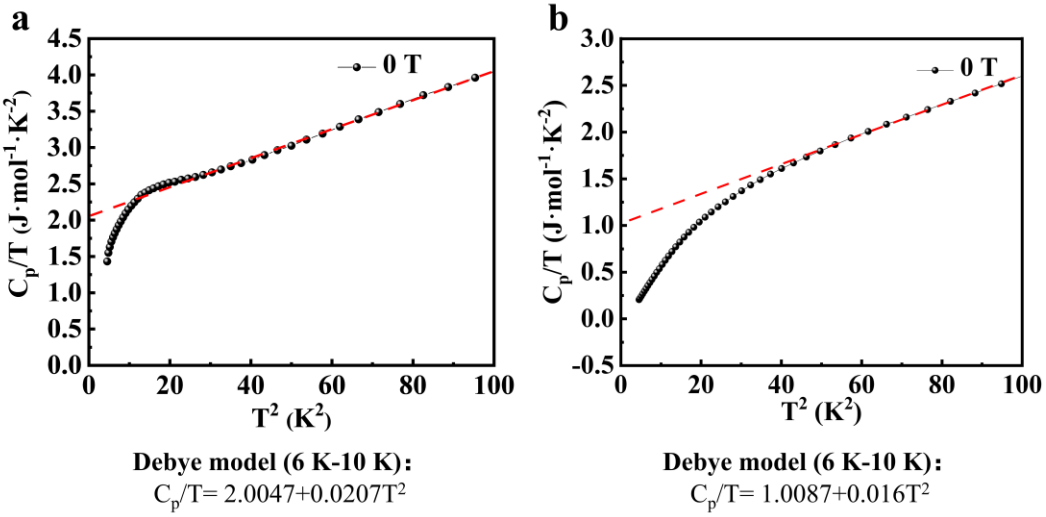

Figure S4. Curve fitting of C_p/T vs T^2 in the range of 6-10 K based on Debye model for $Cs_4BiFeBr_{10}$ (**a**) and $CsFeBr_4$ (**b**) single crystals, respectively.

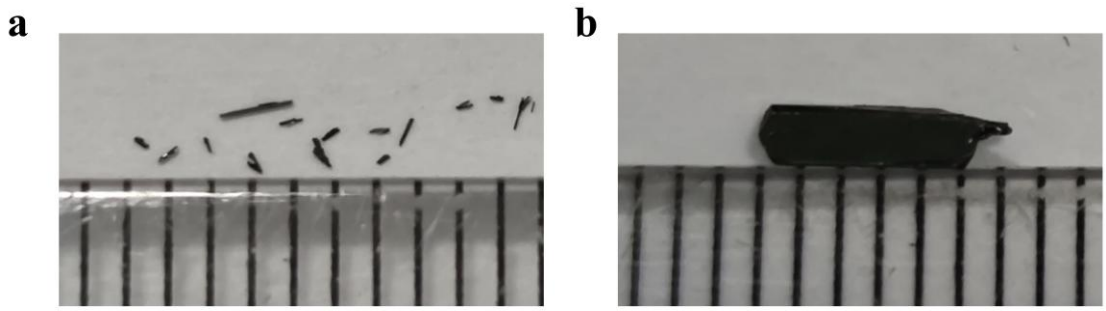

Figure S5. a, the synthesized $Cs_4BiFeBr_{10}$ single crystals; **b**, the synthesized $CsFeBr_4$ single crystals.

Table S1: A comparison of the structural parameters of the two magnetic exchange paths in $Cs_4BiFeBr_{10}$ with those of the similar Cu-based antiferromagnetic systems.

		Distance of Br-Br	Angle of Fe-Br···Br	Angle of Br···Br-Fe	Torsion angle of Fe-Br···Br-Fe	
$Cs_4BiFeBr_{10}$	J_1	3.83 Å	147.6°	147.6°	0°	
	J_2	4.09 Å	92.6°	141°	58.3°	
		Distance of Br-Br	Angle of Cu-Br···Br	Angle of Br···Br-Cu	Torsion angle of Cu-Br···Br-Cu	2J/k (K)
$C_8H_{20}N_2O_2CuBr_4$		3.82 Å	140°	151.5°	53°	-42.6
$C_{10}H_{14}N_6O_5CuBr_4$		4.07 Å	92.3°	148.6°	7.6°	-20.4

Table S2: A comparison of the structural parameters of the two magnetic exchange paths in $CsFeBr_4$ with those of the similar Cu-based antiferromagnetic systems.

		Distance of Br-Br	Angle of Fe-Br···Br	Angle of Br···Br-Fe	Torsion angle of Fe-Br···Br-Fe	
$CsFeBr_4$	J_1	3.78 Å	143.4°	143.4°	0°	
	J_2	4.25 Å	85.3°	117.1°	65°	
		Distance of Br-Br	Angle of Cu-Br···Br	Angle of Br···Br-Cu	Torsion angle of Cu-Br···Br-Cu	2J/k (K)
$C_8H_{20}N_2O_2CuBr_4$		3.82 Å	140°	151.5°	53°	-42.6
$C_{10}H_{16}N_4I_2O_2CuBr_4$		4.23 Å	95°	129°	98°	-1.15